Engineering interfacial structure in "Giant" PbS/CdS quantum dots for photoelectrochemical solar energy conversion

Lei Jin[a], Gianluca Sirigu[b], Xin Tong[a,c], Andrea Camellini[b], Andrea Parisini[d], Giuseppe Nicotra[e], Corrado Spinella[e], Haiguang Zhao[a,*], Shuhui Sun[a], Vittorio Morandi[d], Margherita Zavelani-Rossi[f], Federico Rosei[a,g,*], Alberto Vomiero[h,*]

[a] Institut National de la Recherche Scientifique, 1650 Boulevard Lionel-Boulet, Varennes, Québec, Canada J3X 1S2
[b] Dipartimento di Fisica, Politecnico di Milano, piazza L. da Vinci 32, 20133 Milano, Italy
[c] School of Chemistry and Material Science, Guizhou Normal University, Guiyang 550001, China
[d] CNR IMM Section of Bologna, Via Gobetti 101, 40129 Bologna, Italy
[e] CNR-IMM headquarters, Zona industriale strada VIII n.5, 95121 Catania, Italy
[f] Dipartimento di Energia, IFN-CNR, Politecnico di Milano, via Ponzio 34/3, 20133 Milano, Italy
[g] Institute for Fundamental and Frontier Science University of Electronic Science and Technology of China, Chengdu 610054, PR China
[h] Department of Engineering Sciences and Mathematics, Luleå University of Technology, 971 98 Luleå, Sweden

The interfacial structure in "giant" PbS/CdS quantum dots (QDs) was engineered by modulating the Cd:S molar ratio during in situ growth. The control of the gradient interfacial layer could facilitate hole transfer, regulate the transition from double- to single-color emission, as a consequence. These QDs are optically active close-to-the near-infrared (NIR) spectral region and are candidates as absorber materials in solar energy conversion. Photoinduced charge transfer from "giant" QDs to electron scavenger can still take place despite the ultra-thick (~5 nm) shell. The hybrid architecture based on a TiO_2 mesoporous framework sensitized by the "giant" QDs with alloyed interface can produce a saturated photocurrent density as high as ~5.3 mA/cm^2 in a photoelec-trochemical (PEC) cell under 1

Sun illumination, which is around 2 times higher than that of bare PbS and core/thin-shell PbS/CdS QDs sensitizer. The as-prepared PEC device presented very good stability thanks to the "giant" core/shell QDs architecture with tailored interfacial layer and a further coating of the ZnS shell. 78% of the initial current density is kept after 2-h irradiation at 1 Sun. Engineering of electronic band structure plays a key role in boosting the functional properties of these composite systems, which hold great potential for H_2 production in PEC devices.

Keywords:
Photoelectrochemical
Giant quantum dot
PbS
CdS
Core/shell

1. Introduction

Harvesting energy directly from solar radiation provides an attractive approach towards addressing the increasing demand for clean energy, with minimal environmental impacts [1]. Photoelectrochemical (PEC) cells, which directly convert sunlight into electric power or chemical fuels such as hydrogen (H_2) are considered a promising route for clean and sustainable energy harvesting [1g,2]. Early studies on photoelectrode materials for PEC cells have been focused on TiO_2 and ZnO because of their appropriate energy band position and stability [3]. However, due to their relatively large bandgap of about 3.0–3.2 eV [4], their photoactivation requires ultraviolet (UV)-light, which accounts for only ~5% of the incoming solar energy on the Earth's surface. To enhance the solar energy conversion, it is necessary to extend the light absorption edge of the photoelectrodes. Semiconductor quantum dot (QD) sensitization has recently been studied intensively thanks to their unique size- and shape-tunable optical properties, including efficient broadband absorption [5,6]. Among various kinds of QDs, lead chalcogenide QDs have large exciton Bohr radius (e.g. 18 nm for PbS) and small bulk energy band gaps (e.g. 0.41 eV for PbS), thus allowing quantum confinement in relatively large sized QDs, together with tunable near-infrared (NIR) absorption and emission [7,8,9], providing potential applications in solar cells [9,10,11] and PEC H_2 generation [12,13,14].

Unfortunately, due to their large surface-to-volume ratio, the optical properties of colloidal PbS QDs are very sensitive to their surface chemical conditions (surface ligands, surface oxidation, surface etching, etc.), moisture, oxygen, temperature and/or light [15]. Such

* Corresponding author.
E-mail addresses: haiguang.zhao@emt.inrs.ca (H. Zhao), rosei@emt.inrs.ca (F. Rosei), alberto.vomiero@ltu.se (A. Vomiero).

Received 14 August 2016;
Received in revised form 13 October 2016;
Accepted 15 October 2016
Available online 21 October 2016

sensitivity contributes to the presence of surface traps/defects, leading to a high density of recombination centers, and hence a considerable decrease of chemical/photo-stability [14,16]. Recent studies revealed that the chemical/photo-stability of conventional colloidal QDs can be improved by post-growth of a robust thick CdS inorganic shell via successive ionic layer adsorption and reaction (SILAR) [12,13]. This thick CdS shell inhibits surface oxidation and the formation of surface traps of PbS core due to better surface passivation and isolation from their environment [17,18]. However, *in situ* synthesized QDs with thick CdS passivation layer grown via solid-state SILAR suffer from precise control over QD coverage, high charge recombination due to the possible presence of interfacial traps, and is highly time-consuming [12,19,20]. These issues can be addressed by using in-solution pre-synthesized QDs to sensitize the mesoporous films in PEC systems [21]. Size-tunable thick-shell QDs with high quantum yield (QY) and narrow size distribution can be synthesized via an organometallic approach in an organic solvent, introducing surface ligands to passivate the QD surface [22]. A relatively thick shell (in general 3–5 nm thick) [23,24] can efficiently isolate the core material from the QD's surface chemistry and the surrounding chemical environment [23,25,26,27]. However, the sharp interface in type I PbS/CdS core/shell structures may contribute to unwanted confinement of charge carriers and the interfacial defects caused by the 2% lattice mismatch between the rock salt (RS) crystal structure of the core and zinc blende (ZB) structure of the shell [28,29], hindering charge dissociation and transport for solar energy conversion [30,31]. Engineering the electronic band alignment and interfacial structure to balance electron transfer and surface passivation is therefore required. We have recently demonstrated a hole blockade interfacial layer between the core and shell, leading to double color emission in "giant" QDs [22]. This opens the possibility to optimize QD structure to simultaneously maximize carrier transport and surface passivation. By creating a ternary concentration-gradient interfacial layer between the PbS core and the CdS shell, the charge transfer could be facilitated [23,25], due to the partial leakage of the exciton into the shell, as seen for CdS_xTe_{1-x} [32], $Cd_xZn_{1-x}S$ [33], PbS_xSe_{1-x} [34], and $CdSe/Cd_xZn_{1-x}S$ [35].

In the present investigation, we report new insight into the synthesis of "giant" PbS/CdS QDs with engineered interfacial layer, demonstrating the possibility to fine tune the hole transfer dynamics by controlling the core/shell interface. Interface modulation leads to a transition from double- to single-color emission, as a consequence of the different charge dynamics between a graded and an abrupt interface. By using high-resolution scanning transmission electron microscopy (HR-STEM), we provide evidence of the presence of Pb in single-emitting QDs. In addition, the photoinduced charge transfer behavior, which is essential for practical exploitation of these systems in PEC devices, was investigated by photoluminescence (PL) and ultrafast pump-probe spectroscopy by monitoring the steady-state PL intensity, PL decay and exciton dynamics in a system composed of "giant" QDs and methyl-viologen chloride (MV^{2+}), an electron scavenger. We find that charge transfer can still take place in the thick-shell QDs, although the injection rate is lower, compared to systems with no or very thin shell ($10^5\ s^{-1}$ vs $10^6\ s^{-1}$ in Refs. [17,36]). The PEC H_2 generation investigation demonstrates that a standard mesoporous TiO_2 thick film sensitized by the "giant" QDs with alloyed interface via electrophoretic deposition (EPD) [37] can produce a saturated photocurrent density as high as 3.8 mA/cm^2 under simulated sunlight (AM 1.5 G, 100 mW/cm^2). By engineering the interfacial layer in giant QDs, single-emitting QDs present better stability and higher PEC current density than double-emitting QDs as a consequence of facilitated hole transfer from core (all excited electrons that are delocalized along the core and the shell, due to a quasi-type-II level alignment [38] of the system), consistent with the charge transfer investigation through PL and pump-probe experiments. The atomic-sized halide ligand provides the capacity to improve surface passivation, boosting the current density to 5.3 mA/cm^2 (40% increases) which shows only 22% drop after 2 h irradiation at one Sun intensity (AM 1.5 G, 100 mW/cm^2).

2. Result and discussion

2.1. Synthesis and characterization of "giant" core/shell QDs

PbS/CdS core/thin-shell QDs were first synthesized by starting from pure PbS QDs and inducing the formation of the thin CdS shell through cation exchange [39,40]. They were subsequently used to grow "giant" QDs by SILAR approach by sequentially applying monolayers of inorganic shells (details of the synthesis are reported in Supporting Information (SI) and in Refs. [24,41]). The starting PbS/CdS core/thin-shell QDs after cation exchange, used for the synthesis of the "giant" QDs, have a PbS core of 1.2 nm in diameter and a 1.8-nm-thick CdS shell. The diameter of the core and the thickness of the shell were calculated based on the overall particle size observed through transmission electron microscopy (TEM) images (Fig. S1) and the Pb:Cd molar ratio obtained from inductively coupled plasma-optical emission spectrometry (ICP-OES, Fig. S2) [22,39]. The thin shell made the QDs thermally stable enough for further CdS shell growth at high temperature (240 °C), without degrading their peculiar structural/optical properties (Fig. S3). Simple control of precursor stoichiometry between the Cd and S (from 1:1 to 1:0.8) during the growth of "giant" QDs via SILAR enabled the possibility to control the double/single-color-emitting QDs, which might be related to the modification of the interfacial structure between the core and the shell in the "giant" system.

TEM (Fig. 1a and b) imaging gives a direct view of the morphology and narrow size distribution of PbS/CdS core/shell "giant" QDs with an overall diameter of ~(12.1 ± 0.5) nm for sharp interface QD (Cd:S molar ratio 1:1) (see Fig. S1d) and ~(11 ± 0.5) nm for alloyed interface QD (Cd:S=1:0.8) (see Fig. S1e). The larger overall size of double-emitting QDs with respect to single-emitting QDs is consistent with the higher amount of S during the SILAR. Based on the overall diameter of core/shell QDs estimated from TEM and Pb:Cd molar ratio determined by ICP-OES, the average PbS core radius was estimated to be ~0.6 nm in both single/double-color-emitting "giant" QDs (Table S1). After 8-cycles SILAR, the shell thickness of double-emitting QDs is around 5.5 nm and that of single-emitting QDs is around 4.9 nm.

In this work, a particular effort was devoted to finding an experimental demonstration, by STEM techniques, of the presence of a residual PbS core inside the "giant" CdS QDs. To this end, we performed energy dispersive X-ray spectrometry (EDX) investigations using a large area silicon drift detectors (SDD) EDX detector mounted on a Cs-probe-corrected STEM equipped with a high brightness cold field emission gun. In previous work (see Fig. S4 in Ref. [22]), we demonstrated through EDX spectra simulations of a 1 nm PbS core inside a 10 nm CdS QD that only in STEM mode with a 0.1–1 nm sized focused beam, exactly positioned over the particle core, the presence of Pb could be revealed. Experimentally, this beam positioning, as well as the stability of the core and the overall QD under the intense and prolonged electron irradiation, is very critical.

The results of these STEM and EDX combined investigations are summarized in Fig. 1c and d. A high-resolution high angle annular dark field (HAADF) STEM image of a QD (Fig. 1c) clearly shows the crystalline lattice of CdS and a bright triangular central region. As the image contrast in HAADF-STEM also depends on the atomic number (Z-contrast) [42], we used a very high collection inner semi-angle of 130 mrad (β) to enhance the compositional contrast [43] and avoid the coherent effects of elastic scattering almost entirely thermally diffused [44]. This solution, and the possibility to use a high illumination angle of 33 mrad, guaranteed by the presence of the Cs corrector, allowed us to obtain an image with high signal to noise ratio (SNR), where regions of higher intensity may indicate the presence of a heavier QD core, as shown in the bright triangular central region in Fig. 1c. To determine the core composition, an EDX spectrum acquired in a small

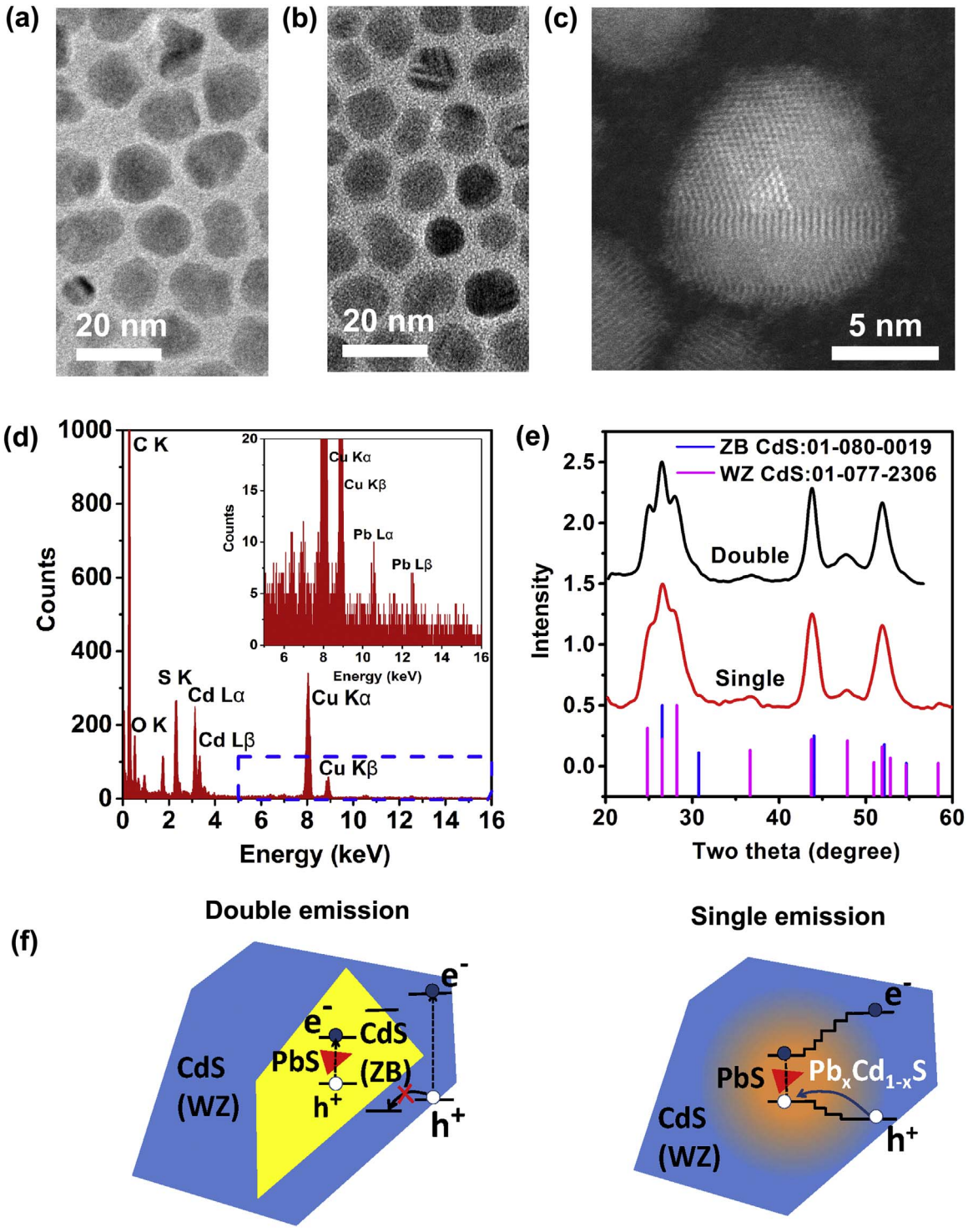

Fig. 1. TEM images of (a) double-emitting and (b) single-emitting "giant" QDs. (c) HAADF-STEM image of a "giant" QD. (d) A portion of an EDX X-ray spectrum obtained on a square region around the bright triangular central area of the QD in (c). Inset: the blue box marked region of the spectrum in (c) is displayed on an expanded scale. (e) XRD patterns of "giant" QDs. The Joint Committee on Powder Diffraction Standards (JCPDS) card files for CdS (01 080 0019, blue for ZB and 01-077-2306, magenta for Wurtzite (WZ)) are shown for identification. (f) A schematic structure and electronic band structure of double-emitting (left) and single-emitting "giant" QDs (right), highlighting the PbS core (red) the external ZB shell (azure) and the interface region, in the case of sharp (WZ, yellow) and graded interface.

square area around the bright triangular central region was recorded (Fig. 1d). In this spectrum, the C, S, Cd and Cu (from the supporting grid) are the main X-ray peaks, however, weak but clear Pb L peaks are detected in this region (inset of Fig. 1d), indicating the presence of Pb in the QD core. It is worth nothing, that owing to the critical points previously described,, it is not always possible to detect the presence of the Pb L peaks during these experiments. Finally, if the bright central areas visible in QDs HAADF-STEM images like that in Fig. 1c are identified with the PbS core projections, the resulting dimensions of the PbS cores are consistent with the above-reported estimation.

The crystal structure of the QDs was further characterized by X-ray diffraction (XRD, Fig. 1e). The core/shell nanocrystals after cation exchange shift from an RS to a ZB CdS-like pattern [17,22]. After 8 cycles of CdS coating, the overall diffraction pattern exhibits reflections

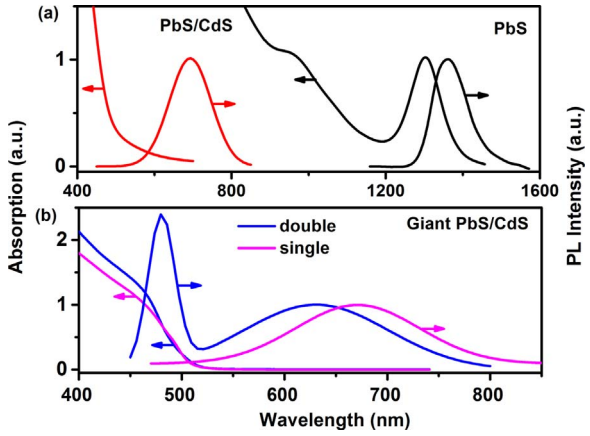

Fig. 2. Absorption and PL spectra of (a) pure PbS and core/thin-shell PbS/CdS QDs after cation exchange and (b) double-emitting and single-emitting PbS/CdS core/thick-shell "giant" QDs after SILAR.

from both CdS hexagonal WZ and CdS ZB structure [45,46]. irrespective of the Cd:S molar ratio used during the SILAR reaction (Fig. 1e), consistent with HAADF high-resolution STEM investigations (Fig. S4). However, based on the further quantitative analysis (Table S2 and Fig. S5, SI), the relative intensity of peaks related to ZB in double-emitting QDs is almost double compared to that in the single-emitting QDs. This observation is in perfect agreement with the explanation of the double emission as a consequence of the presence of a thick ZB shell acting as a hole-blocking layer [22,45]. No clear reflection from PbS was visible in the XRD pattern of PbS/CdS QDs, even after the growth of a thin CdS shell, due to the very small PbS content (0.1% in vol. in the "giant" system).

The absorption and PL spectra of the QDs with or without SILAR treatment are reported in Fig. 2. The starting bare PbS QDs show a clear and narrow first-exciton peak at 1310 nm, indicating a narrow size distribution, consistent with the TEM observation (Fig. S1d and e). The absorption spectrum of core/thin-shell QDs after cation exchange shifts to lower wavelengths due to the shrinking of the PbS core (Fig. 2a). A Cd:S molar ratio equal to 1:1 during SILAR results in a double-color emission, with two peaks at 630 nm and 480 nm, respectively (Fig. 2b, blue PL signal). When the Cd:S molar ratio is set to 1:0.8, the "giant" QDs show a typical single emission at 670 nm (Fig. 2b, pink PL signal). As previously reported [17,39]. the peak at 480 nm originates from the CdS shell emission, and the one at 630 nm comes from the PbS core. PbS emission has a lifetime in the μs scale, which is typical for PbS QDs [36]. In single-emitting QDs, the band at 670 nm has a lifetime in the μs scale, suggesting the same origin as the double-emitting QDs.

We previously elucidated the mechanism of double-color emitting QDs via pump-probe spectroscopy, which is due to the presence of a core/ZB shell/WZ shell structure (Fig. 1f) [22], in which the ZB shell acts as "hole-blocker" due to a difference in band offsets between ZB and WZ CdS [47]. Now, we can control the interfacial potential barrier between the core and the external shell by modulating the Cd:S molar ratio during SILAR, allowing us to tailor the hole transfer and the double-to-single-color transition in "giant" QDs. When the Cd:S molar ratio is 1:1, at the high reaction temperature, the Cd-oleate reacts with S and does not replace the Pb in the PbS core (cation exchange), forming an abrupt core/shell interface consisting of a PbS core and a CdS ZB shell. At Cd:S molar ratio higher than 1:0.8, the excess Cd still undergoes the cation exchange reaction, which releases free Pb cations. These Pb cations can further react with S to form a $Pb_XCd_{1-X}S$ alloy, leading to a graded interface (see the scheme in Fig. 1f, right). As shown in Fig. S3, annealing at high temperature (240 °C) in a Cd-oleate-free environment does not induce significant changes in the PL of QDs after cation exchange, suggesting that the PbS core keeps its original size and composition. A clear blue shift is recorded, instead, by dispersing the QDs in Cd-oleate precursors at 240 °C. This behavior actually confirms that, even with a thicker shell around the PbS, the cation exchange still can undergo if an excess of Cd-oleate is present. The PL peak of PbS core in single-emitting "giant" QD presents a red shift compared to that of double-emitting "giant" QDs, indicating the possible existence of alloyed $Pb_XCd_{1-X}S$ interfacial layer, leading to exciton leakage [45]. The probable presence of the alloyed interfacial layer provides an energy gradient, endowing the fast release of the photogenerated hole from the CdS WZ shell to the PbS core, inhibiting direct exciton radiative recombination within the CdS shell and leading to the single emission of "giant" QDs, while the abrupt core/shell interface leads to double emission [45].

2.2. Charge dynamics of QDs coupled with electron scavenger

To further understand the optical properties of "giant" QDs, we examined their charge transfer behavior by using an electron scavenger, namely MV^{2+}. The redox energy level of MV^{2+} is around 4.06 eV versus the vacuum [31], which is favorable for electron injection from both the PbS and CdS investigated here. The absorption of MV^{2+} below 350 nm does not overlap with any PL band of the QDs, excluding any possible energy transfer from the QDs to MV^{2+} [31]. The QD sample at the same concentration (details for identifying the concentration are reported in SI and Fig. S2) were mixed with MV^{2+}, then the charge transfer behavior was investigated by static and transient PL spectra. Taking into account the experimental error, the concentration ratios of MV^{2+} and QDs for single- and double-emitting QDs can be regarded as similar. The PL intensity is observed to decrease (Fig. 3a and b) with the increasing concentration of the electron scavengers. Such emission was quenched after the introduction of MV^{2+}, due to photo-excited charge transfer processes, and the higher quenching rate suggests more efficient electron transfer [31]. To quantitatively study the PL quenching behavior, we considered the PL intensity ratio φ:

$$\varphi = I/I_0$$

where I_0 and I are the integrated PL intensities observed without and with quenchers (MV^{2+}) in solution, respectively. As shown in Fig. 3c, in double-emitting QDs, the PL quenching of the peak attributed to the PbS core is much more intense than the peak attributed to the CdS shell. This is possibly due to the rapid radiative recombination (several ns), which occurs in the CdS shell, because charge transfer from the shell cannot effectively compete with the emission process in terms of time scale [17]. On the other hand, the PbS in double-emitting QDs presents more efficient quenching with respect to PbS core in single-emitting QDs (Fig. 3c). This can be explained by examining the structural features of QDs. In case of single-emitting QDs, an alloyed interfacial layer could provide an energy gradient. Once the photo-generated electron of CdS is captured by MV^{2+}, the photo-generated hole of CdS could quickly migrate to the PbS core to recombine with the electron of PbS, contributing to the core emission. In double-emitting QDs, instead, the ZB shell acting as "hole blocker" confines the hole in the CdS shell, which can no longer contribute to PbS emission. Moreover, electrons from PbS can tunnel through the CdS barrier, being captured by MV^{2+} at the surface of the QDs.

To understand the phenomenon, we investigated the fluorescence decay of the "giant" QDs after the introduction of MV^{2+}, by analyzing the charge transfer rate constants (k_{et}) derived from the fluorescence lifetime. The decay curves of the PL peak corresponding to PbS core and CdS shell, which varied with the concentration of MV^{2+}, were well fitted with a three-component (PbS emission) and two-component (CdS emission) exponential decay, respectively, shown on a semi-logarithmic plot (Fig. 4a, b and c). To estimate the charge transfer rate constant, the average PL lifetime was calculated fromτ_1, τ_2 (and τ_3), the characteristic decay times of the two (or three)-component decay. The intensity-weighted average lifetime $<\tau>$ is estimated as follows:

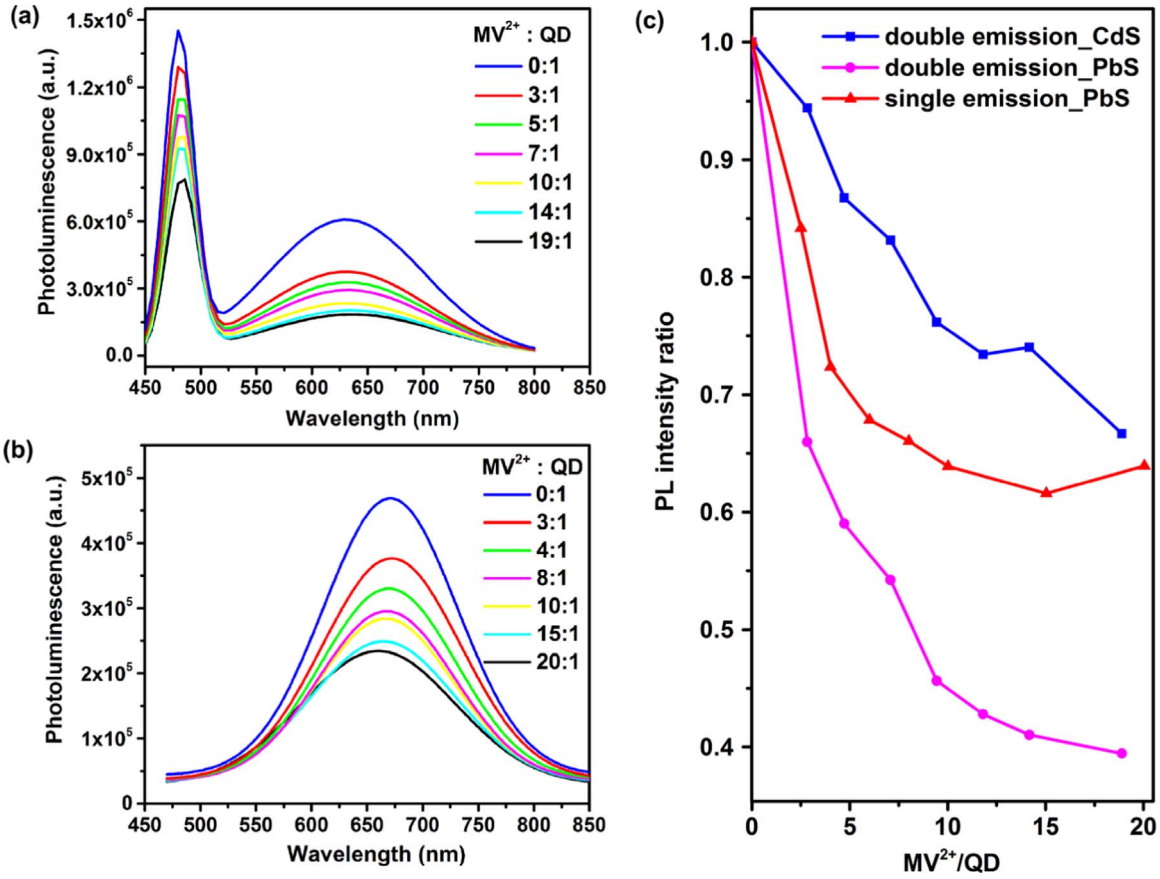

Fig. 3. PL of (a) double-emitting and (b) single-emitting "giant" QDs with the introduction of MV^{2+} as a function of MV^{2+}/QD concentration ratio. (c) PL intensity ratio of PbS core emission in double-emitting and single-emitting "giant" QD for MV^{2+}/QD concentration ratio equal to the ones shown in (a) and (b).

$$<\tau> = \frac{\sum a_i \tau_i^2}{\sum a_i \tau_i}$$

Where a_i are the coefficients of the fitting of PL decay (i=1, 2 and i=1, 2, 3 for double/tri-exponential decay, respectively). The average PL lifetime of the core largely decreased from around 1330 ns (MV^{2+}: QD =0: 1) to 1040 ns for double-emitting QDs with the addition of MV^{2+}(MV^{2+}: QD =18.9: 1); a similar trend was also found in the single-emitting QDs (Fig. 4a, b). The average PL lifetime of CdS was ~13 ns without the addition of MV^{2+}(Fig. 4c), which is within the range reported for CdS QDs [48]. The charge-transfer rate constant (k_{et}) was then estimated using the following equation [49]:

$$k_{et} = \frac{1}{<\tau>_{QD/MV^{2+}}} - \frac{1}{<\tau>_{QD}}$$

Where $<\tau>_{QD/MV^{2+}}$ and $<\tau>_{QD}$ are the average PL lifetimes of the QD/MV^{2+} and QDs systems, respectively. Fig. 4d shows the variation of k_{et} with MV^{2+} concentration. The charge-transfer rate of the PbS core significantly increases with the increase of MV^{2+} concentration up to reach a value of 2×10^5 s^{-1} (Fig. 4d), which is similar to the k_{et} of single-emitting QDs. On the other hand, as shown in Fig. 4d, the charge transfer rate of CdS emission (2×10^7 s^{-1}) is 100 times faster than that of PbS.

In general, photoexcited charge transfer from QDs to charge scavengers relies on geometric factor, time scale and band alignment [17,36,50]. In the "giant" QDs, the PbS QDs are surrounded by the thick CdS shell, which largely slows down the charge transfer from the core. To better understand the role of the shell, we performed pump-probe measurements with a time resolution of about 100 fs collecting the differential transmission ΔT/T spectra for different pump-probe delays. We adjusted the pump photon energy at the bandgap of CdS so as to disregard exciton thermalization toward the band-edge and focus on exciton recombination and charge transfer. We used low pump fluences so as to have an average number of exciton per dot $<N>$ lower than one and avoid multiexciton processes. ΔT/T spectra (Fig. S6 a and b in SI) show a positive signal assigned to bleaching of CdS states, by comparison with the absorption spectrum of the samples (Fig. S6 in SI and Fig. 2b). In fact, the absorption spectra are dominated by the CdS, as PbS contribution cannot be detected due to the high ratio between the volume of the shell and the total volume of "giant" QDs [51], and MV^{2+} shows no absorption in the 300–700 nm range [52]. ΔT/T signal from CdS, however, reflects the behavior of all excited electrons that are delocalized along the core and the shell, due to a quasi-type-II level alignment of the system [22]. The effect of electron scavenger can be noted in ΔT/T spectra, which show a reduction of the bleaching signal when MV^{2+} is mixed to QDs (more evident for single-emitting QDs, but also present in "giant" QDS, Fig. S6a and b), while the photoinduced absorption could not be detected due to formation of MV^{2+} radical [31], because it overlaps with photoinduced absorption from defects states. More evidence of the role of the charge scavenger can be observed in ΔT/T bleaching dynamics (Fig. 5): the presence of the MV^{2+} causes a faster decay of the signal both in the single and double emitting QDs, which is a further unambiguous signature of charge transfer [31].

ΔT/T bleaching kinetics allows also for an estimation of the charge transfer rate. ΔT/T in our system reflects the population of photo-excited electrons, whose decay is a consequence of exciton recombination in bare QDs samples and of exciton recombination and charge transfer in QDs mixed with MV^{2+}. We fitted the kinetics and best results were obtained using a bi-exponential function. Using the intensity weighted average lifetime defined above [31,36,53], we obtain a charge transfer rate of about 2×10^7 $s^{-1}$for the single-emitting "giant"

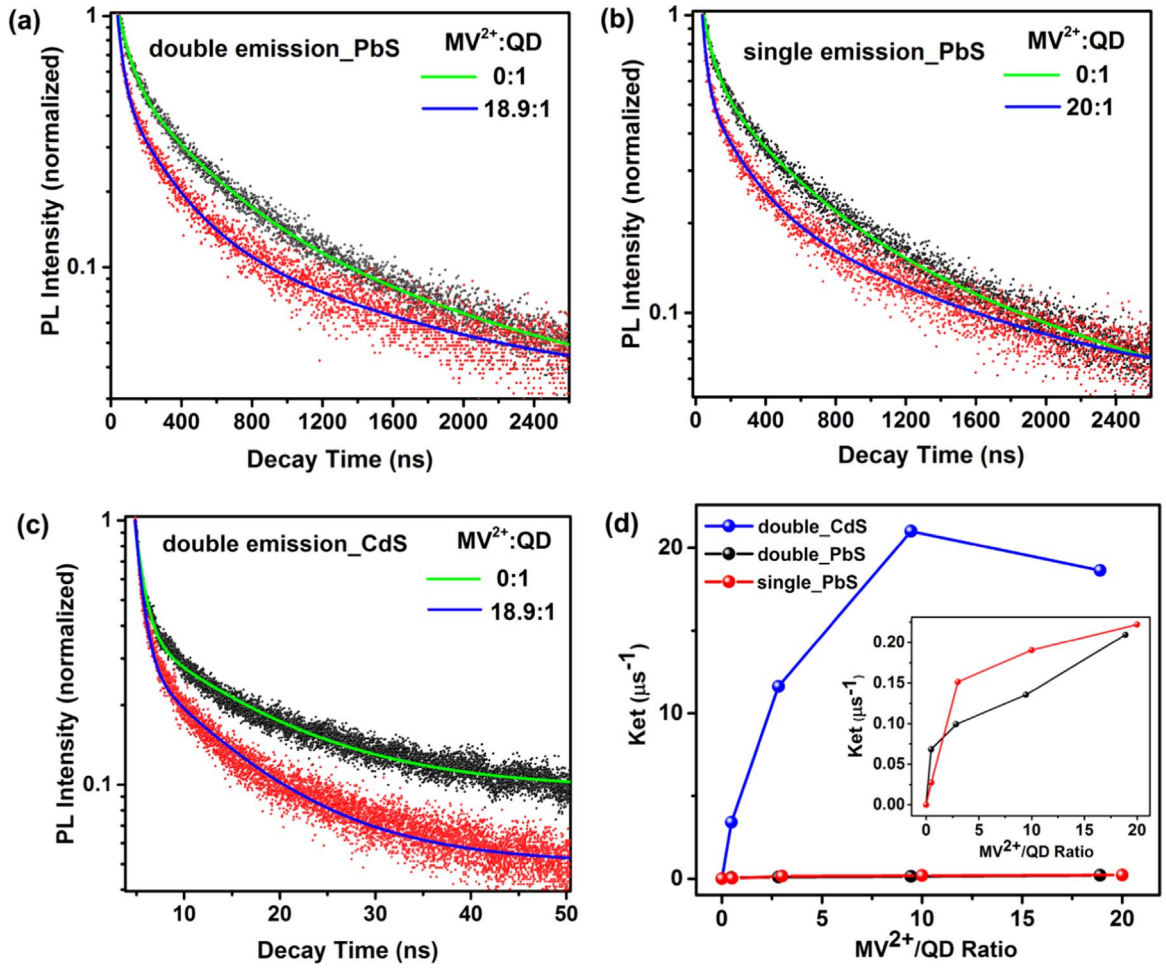

Fig. 4. Typical PL decay curves vary without and with the introduction of MV^{2+} for (a) PbS core emission (630 nm) in double-emitting "giant" QDs (b) single-emitting "giant" QDs (670 nm), (c) CdS shell emission (480 nm) in double-emitting "giant" QDs. (d) Charge transfer rate constants derived from the fluorescence lifetime, k_{et} varied with MV^{2+} concentration. All QDs were dispersed in toluene and PL measurements were carried out at ambient temperature with a laser of 444 nm.

QD and about $3\times10^{7}\ s^{-1}$ for the double-emitting "giant" QD. These results are consistent with the method proposed by Senty et al. in Ref. [54] for the evaluation of the electron transfer rate behavior as a function of the carrier concentration. We found the same values for time delays longer than few hundreds of picoseconds (while they are one order of magnitude higher for shorter time delays, corresponding to higher carrier concentrations). These results are in agreement with data obtained from PL analyses and show that on the short ns time

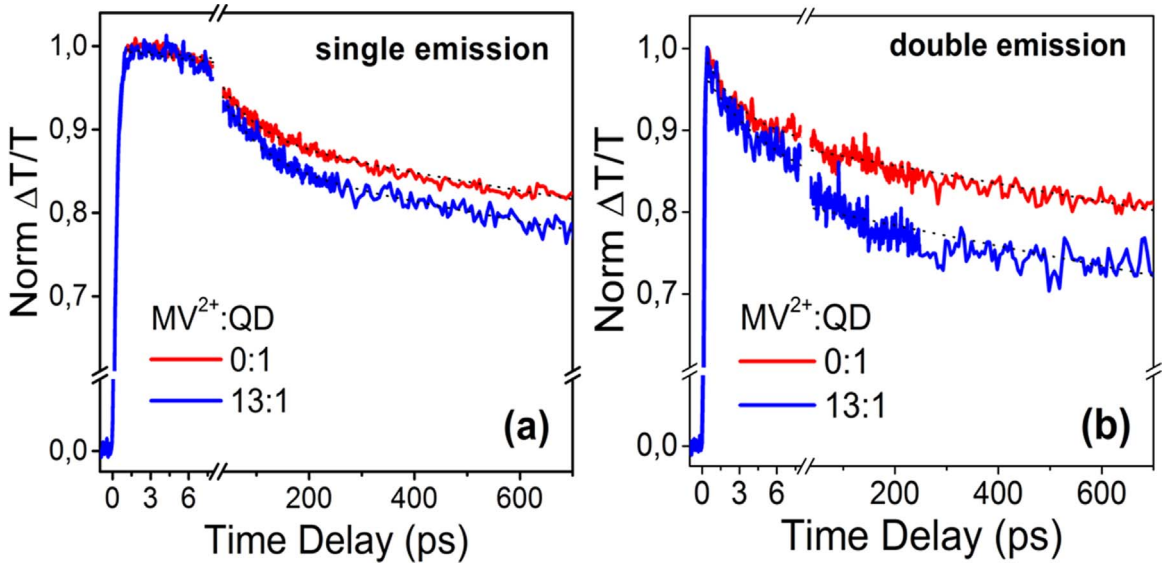

Fig. 5. ΔT/T dynamics for $< N > = 0.4$ for "giant" QDs without (red curves) and with MV^{2+}(blue curves) for (a) single-emitting QDs and (b) double-emitting QDs, at CdS band probe energy (500 nm), together with fit (dotted lines).

scale range electron transfer is mediated by the CdS shell. The charge transfer is still effective (Fig. S6c and d in SI) also in the multiexciton regime.

Due to the passivation of CdS thick shell, the electron transfer rate from the core is largely slowed down, typically much slower than in the pure PbS (k_{et} of 10^7 s^{-1}) or in thin-shell PbS/CdS QDs/MV^{2+}(k_{et} of 1~8×10^6 s^{-1}) [17]. With respect to PbS, CdS shows much faster transfer rate, due to the shorter distance from the MV^{2+}, the larger driving force, ΔG (energy difference between the acceptor and donor systems) and the absence of any additional energy barrier [36]. The less efficient quenching of CdS shell with respect to PbS core in double-emitting "giant" QDs, is possibly due to the rapid radiative recombination (several ns) in CdS shell, because charge transfer from the shell cannot effectively compete with the emission process in terms of time scale. However, the above results indicate that efficient charge transfer is still possible. By controlling the interfacial structure of "giant" QDs, the hole transfer dynamic could be engineered for the potential use of PbS/CdS "giant" QDs in electronic and optoelectronic devices.

2.3. PEC performance

To demonstrate the potential of "giant" QDs for solar energy conversion applications, they were loaded into TiO_2 mesoporous film through EPD [37]. Additional ZnS 2-cycle SILAR deposition was added to deposit a protective coating at QD surface. The PEC activity of the TiO_2/QDs system toward the H_2 evolution reaction (HER) was studied by employing a three-electrode electrochemical cell configuration [13]. A set of linear-sweep voltammograms with respect to the reversible hydrogen electrode (RHE) ($V_{RHE}=V_{Ag/AgCl}+0.197+pH\times(0.059)$) [12,55] was recorded on different photoanodes in the dark and under simulated solar illumination (AM 1.5 G, 100 mW/cm^2). The photocurrent density in light gradually grows with the increase in voltage, until a saturated current density is obtained (Fig. 6b). Compared to bare single emitting QD-sensitized photoanode (Fig. S7), the photoanode with ZnS capping layer presents a 3-fold enhancement of the saturated current density, as high as 3.8 mA/cm^2 (Fig. 6b), which could be ascribed to the significantly reduced charge recombination by the interposition of an intermediate layer as a ZnS coating [56]. For double-emitting QDs, a saturated current density of 3 mA/cm^2 is obtained, which is lower than values obtained for single-emitting QDs. This discrepancy may be understood by considering the possible scheme of PEC device as illustrated in Fig. 6a. In the double-emitting QDs, the ZB CdS layer lying between PbS core and WZ CdS external layer can block the hole transfer from the PbS core. The holes need to tunnel through the ZB CdS layer during PEC reaction; the consequent less efficient hole transfer may contribute to increased charge recombination, and herein the lower saturated current density (Fig. 6b). However, in the single-emitting QDs, the alloy interfacial layer, forming an energy gradient in the electronic band between the core and the shell (dashed stair in Fig. 6a), could allow efficient hole transfer from the core to the electrolyte.

The stability of the PEC systems was investigated under 100 mW/cm^2 AM 1.5 G illumination, with 0.2 V vs. RHE potential applied (Fig. 6c). The photocurrent density of double and single-emitting QD-based PEC cells gradually decrease during illumination, with a drop equal to 55% and 25% of their initial value after 5000 s. Single-emitting QDs present better stability with a drop of 30% even after 2 h. The worse PEC stability observed for double-emitting QD-based PEC cell could be due to the hole-induced self-oxidative decomposition of the metal chalcogenide (detailed explanation is included in Fig. S9 and description there in) [1e], as a consequence of the presence of a thick ZB CdS acting as a hole blocking layer (Fig. 1f, Fig. 6a), which is consistent with the charge transfer investigation discussed above. As shown in Fig. 6d and e, cetyltrimethylammonium bromide (CTAB) was introduced to boost the saturated current density of single-emitting QDs to 5.3 mA/cm^2, which is around 2 times higher than that of bare PbS and core/thin-shell PbS/CdS QDs sensitizer [13] at the same condition (Fig. S8). The 40% increase in saturated current density probably due to a higher injection QY and lower interfacial charge recombination with the electrolyte [57,58]. Significantly, upon illumination on/off, a spike in the photoresponse was obtained for single-emitting QDs with and without ligand exchange (Fig. 6e), indicating efficient charge separation and fast charge transport from QDs to a current collector via TiO_2 networks. As shown in X-ray photoelectron spectroscopy (XPS) (Fig. S10), CTAB atomic-ligand passivation strategy introduced Br^- to cap the surface cations respectively, forming all-inorganic, halide anion-passivated QDs [58]. Applied inorganic CTAB ligand strategies could keep higher carrier mobility and lower the defect density to reduce recombination loss in single-emitting QDs after EPD, as well as better surface passivation, therefore, only 22% current density drop was observed after 2 h as a consequence (Fig. 6c). In fact, the stability of our "giant" QDs is comparable with the best stability in the similar system reported in the literature [59].

3. Conclusions and perspectives

In conclusion, we have synthesized close-to-NIR "giant" PbS/CdS QD by growing very thick inorganic CdS shell (~5 nm in thickness) onto a PbS core (~0.6 nm core radius). Exciton and charge dynamics (specifically, the charge transfer of the hole from the shell to the core) can be controlled by manipulating the core/shell interface, which affects single/dual color emission of "giant" QDs. A detailed investigation of the photoinduced charge transfer confirmed that the electron in the core can delocalize into the shell, and further to the outlayer of QDs, even with ultra-thick shell, after mixing with electron scavenger. These findings are critical for the suitable design of complex systems, with tailored optical and electronic properties for specific applications. We used the "giant" QDs to sensitize a TiO_2 mesoporous photoanode architecture for PEC H_2 production, confirming the results of charge transfer investigation. The PEC stability benefits from the thick protective shell. Due to the close-to-NIR emission, long lifetime and possible photoinduced charge transfer, good reproducibility, PbS/CdS "giant" QDs hold wide potential applications in electronics and optoelectronics. Inorganic ligand strategies could help to improve the PEC behavior of "giant" QDs. Further synthesis of "giant" PbS/CdS QDs with emission ranging from 900 to 1200 nm are ongoing to develop a class of QDs optically active in the NIR region for solar energy and optoelectronic applications.

4. Experimental section

4.1. A detailed description of the experimental methods is available in SI

4.1.1. QD synthesis

PbS QDs were synthesized by using OLA as ligands and PbS/CdS thin-shell QDs were synthesized via a two-step cation exchange procedure [60]. Deposition of CdS layer on PbS/CdS QDs followed the procedure described in Dennis et al. [61] For the synthesis of dual-color-emitting "giant" QDs, the molar ratio of Cd/S is equal, while for synthesizing single-emitting "giant" QDs, the molar ratio of Cd/S is around 1:0.8. The QDs were washed by ethanol and then re-dispersed in toluene.

4.1.2. TiO_2 film preparation

A thin and compact TiO_2 layer was spin coated on FTO-coated glass at 2000 rpm for 60 s by using the commercial solution Ti-Nanoxide BL/SC (Solaronix). Then the films were annealed in air at 500 °C for 30 min after drying and cooled down to room temperature. A blend of active anatase particles (~20 nm) and larger anatase scatter particles (up to 450 nm) paste (18 NR-AO, paste B, from Dyesol) was tape casted, forming a mesoporous film with thickness ~14 μm, as mea-

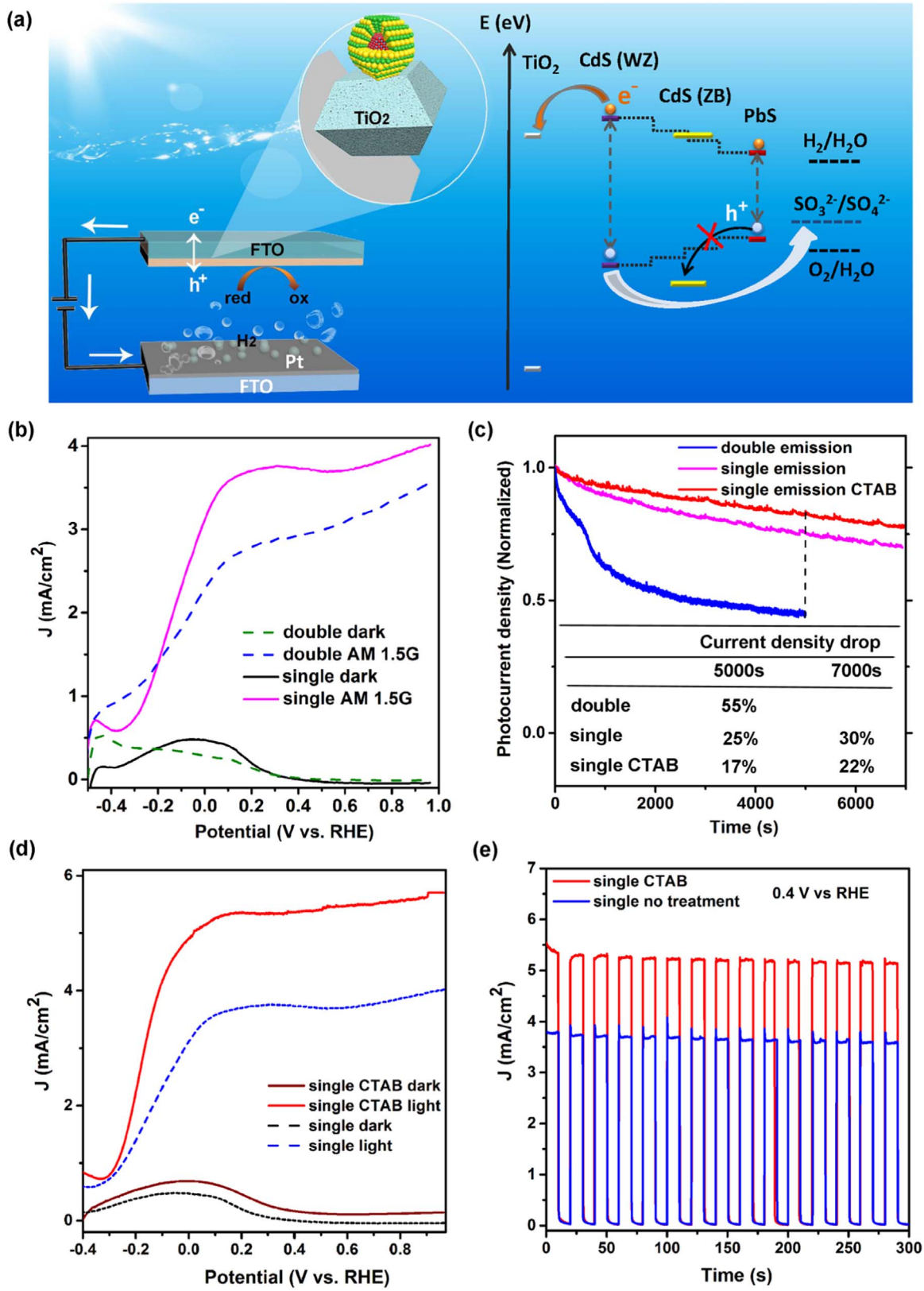

Fig. 6. (a) Scheme of the PEC device. Right: The schematic band structure, the "dashed stair" is corresponding to the alloyed interfacial layer in single-emitting QDs and the ZB CdS is located between PbS core and WZ CdS in double-emitting QDs. The arrows indicate the electron and hole transfer process. (b) Photocurrent density versus the applied voltage (vs. RHE) for the TiO_2/single-emitting QDs/ZnS and TiO_2/double-emitting QDs/ZnS in the dark and under AM 1.5 G illumination at 100 mW/cm^2. (c) Measured current density of sample TiO_2/single-emitting QDs/ZnS (red curve) and TiO_2/double-emitting QDs/ZnS (blue curve) as a function of time (normalized) at 0.2 V vs. RHE under 100 mW/cm^2 illumination with AM 1.5 G filter. Inset table: the current density drop for TiO_2/single-emitting QDs/ZnS and TiO_2/double-emitting QDs/ZnS after 4000 s. Photocurrent density versus (d) the applied voltage (vs. RHE) and (e) time for sample TiO_2/single-emitting QDs without and with CTAB treatment, before applying ZnS SILAR treatment.

sured by contact profilometry.

4.1.3. EPD of the "giant" QDs on the TiO_2 film

A pair of TiO_2/FTO slides vertically immersed in the QDs solution and facing each other with a distance of 1 cm. A voltage of 200 V was applied for 120 min [13]. The samples were then rinsed several times with toluene and dried with N_2 at room temperature. After that the anode was immersed in CTAB methol solution for 1 min and then rinsed by methanol. Later on, two monolayers of ZnS were subsequently deposited using SILAR.

4.1.4. Characterization

Morphology and size distribution (Fig. 1a, b and Fig. S1) of PbS/CdS QDs was characterized by a JEOL 2100F TEM. High-resolution TEM and composition of PbS/CdS single-emitting "giant" QDs were characterized by Cs-probe-corrected JEOL ARM200CF TEM/STEM operated at its full energy of 200 keV, equipped with a cold field emission gun and a 100 mm^2 EDX Silicon drift detector (SDD) named "Centurio" (Fig. 1c and d). XRD was carried out with a Philips X'pert diffractometer using Cu-K_α radiation source (λ=0.15418 nm). XPS was performed in a VG Escalab 220i-XL equipped with a hemispherical analyzer for a Twin Anode X-Ray Source. ICP-OES was carried out with Perkin Elmer Model Optima 7300 DV. Absorption spectra were acquired with a Cary 5000 UV–Vis–NIR spectrometer (Varian) with a scan speed of 600 nm/min. Static and transient fluorescence spectroscopy were taken with a Fluorolog®–3 system (Horiba Jobin Yvon). Pump-probe measurements were performed using a Ti:Sapphire laser system (Coherent LIBRA-HE). The PEC performance of the photoelectrodes was evaluated in a typical three-electrode configuration, with 0.25 M Na_2S and 0.35 M Na_2SO_3 as the sacrificial hole scavengers. All potentials measured with respect to Ag/AgCl were converted to the RHE scale. The photoresponse was measured by using a Sciencetech SLB-300A Compact Solar Simulator Class AAA. Prior to each measurement, light intensity was monitored by a thermopile and the illumination at the surface of the sample was calibrated to ~100 mW/cm^2 with a Solar Reference Detector (NIST-certified Si solar cell) equipped with Power Meter (Sciencetech SOL-METER-D). Typically, the distance between the measured sample and the lamp is around 15 cm.

Acknowledgements

We acknowledge funding from the Natural Science and Engineering Research Council of Canada (NSERC), the Canada Foundation for Innovation (CFI) for infrastructure and its operating funds and the Fonds de recherche du Québec – Nature et technologies (FRQNT) for team grants. L.J. acknowledges FRQNT for Merit Scholarship Program. F.R. acknowledges NSERC for an EWR Steacie Memorial Fellowship. G.S. and M.Z.-R. acknowledge COST Action MP1302-NanoSpectroscopy. A.V. acknowledges Kempe Foundation, Swedish Foundations' Consolidator Fellowship and LTU Labfund program for partial funding. A.P., G.N., C.S. and V.M. acknowledge the project Beyond-Nano (PON a3_00363) at the Beyondnano CNR-IMM laboratory, supported by the Italian Ministry of Education and Research (MIUR). We thank Prof. Ana Tavares for useful discussions during data analysis and manuscript preparation.

Appendix A. Supplementary material

Supplementary data associated with this article can be found in the online version at doi:10.1016/j.nanoen.2016.10.029.

References

[1] (a) G.W. Crabtree, N.S. Lewis, Phys. Today 60 (2007) 37;
(b) X. Chen, L. Liu, F. Huang, Chem. Soc. Rev. 44 (2015) 1861;
(c) M.G. Walter, E.L. Warren, J.R. McKone, S.W. Boettcher, Q. Mi, E.A. Santori, N.S. Lewis, Chem. Rev. 110 (2010) 6446;
(d) T. Wang, J. Gong, Angew. Chem. Int. Ed. 54 (2015) 10718;
(e) X. Chen, S. Shen, L. Guo, S.S. Mao, Chem. Rev. 110 (2010) 6503;
(f) H.M. Chen, C.K. Chen, R.-S. Liu, L. Zhang, J. Zhang, D.P. Wilkinson, Chem. Soc. Rev. 41 (2012) 5654;
(g) M. Grätzel, Nature 414 (2001) 338.
[2] (a) G. Hodes, Nature 285 (1980) 29;
(b) J.A. Turner, Science 285 (1999) 687;
(c) R. van de Krol, Y. Liang, J. Schoonman, J. Mater. Chem. 18 (2008) 2311;
(d) A.G. Pattantyus-Abraham, I.J. Kramer, A.R. Barkhouse, X. Wang, G. Konstantatos, R. Debnath, L. Levina, I. Raabe, M.K. Nazeeruddin, M. Gratzel, ACS Nano 4 (2010) 3374.
[3] A. Fujishima, Nature 238 (1972) 37.
[4] A. Hagfeldt, M. Graetzel, Chem. Rev. 95 (1995) 49.
[5] L.E. Brus, J. Chem. Phys. 79 (1983) 5566.
[6] A.P. Alivisatos, Science 271 (1996) 933.
[7] A.L. Rogach, A. Eychmüller, S.G. Hickey, S.V. Kershaw, Small 3 (2007) 536.
[8] Y. Zhou, D. Benetti, Z. Fan, H. Zhao, D. Ma, A.O. Govorov, A. Vomiero, F. Rosei, Adv. Energy Mater. 6 (2016) 1501913.
[9] I. Concina, C. Manzoni, G. Grancini, M. Celikin, A. Soudi, F. Rosei, M. Zavelani-Rossi, G. Cerullo, A. Vomiero, J. Phys. Chem. Lett. 6 (2015) 2489.
[10] W.U. Huynh, J.J. Dittmer, A.P. Alivisatos, Science 295 (2002) 2425.
[11] I. Robel, V. Subramanian, M. Kuno, P.V. Kamat, J. Am. Chem. Soc. 128 (2006) 2385.
[12] R. Trevisan, P. Rodenas, V. Gonzalez-Pedro, C. Sima, R.S. Sanchez, E.M. Barea, I. Mora-Sero, F. Fabregat-Santiago, S. Gimenez, J. Phys. Chem. Lett. 4 (2013) 141.
[13] L. Jin, B. AlOtaibi, D. Benetti, S. Li, H. Zhao, Z. Mi, A. Vomiero, F. Rosei, Adv. Sci. 3 (2016) 1500345.
[14] Y. Jin-nouchi, T. Hattori, Y. Sumida, M. Fujishima, H. Tada, ChemPhysChem 11 (2010) 3592.
[15] K. Szendrei, M. Speirs, W. Gomulya, D. Jarzab, M. Manca, O.V. Mikhnenko, M. Yarema, B.J. Kooi, W. Heiss, M.A. Loi, Adv. Funct. Mater. 22 (2012) 1598.
[16] S. Hinds, S. Myrskog, L. Levina, G. Koleilat, J. Yang, S.O. Kelley, E.H. Sargent, J. Am. Chem. Soc. 129 (2007) 7218.
[17] H. Zhao, H. Liang, B.A. Gonfa, M. Chaker, T. Ozaki, P. Tijssen, F. Vidal, D. Ma, Nanoscale 6 (2014) 215.
[18] J.M. Pietryga, D.J. Werder, D.J. Williams, J.L. Casson, R.D. Schaller, V.I. Klimov, J.A. Hollingsworth, J. Am. Chem. Soc. 130 (2008) 4879.
[19] H. Lee, H.C. Leventis, S.J. Moon, P. Chen, S. Ito, S.A. Haque, T. Torres, F. Nüesch, T. Geiger, S.M. Zakeeruddin, Adv. Funct. Mater. 19 (2009) 2735.
[20] A. Braga, S. Giménez, I. Concina, A. Vomiero, I. Mora-Seró, J. Phys. Chem. Lett. 2 (2011) 454.
[21] D.R. Baker, P.V. Kamat, Adv. Funct. Mater. 19 (2009) 805.
[22] H. Zhao, G. Sirigu, A. Parisini, A. Camellini, G. Nicotra, F. Rosei, V. Morandi, M. Zavelani-Rossi, A. Vomiero, Nanoscale 8 (2016) 4217.
[23] Y. Chen, J. Vela, H. Htoon, J.L. Casson, D.J. Werder, D.A. Bussian, V.I. Klimov, J.A. Hollingsworth, J. Am. Chem. Soc. 130 (2008) 5026.
[24] H. Htoon, A.V. Malko, D. Bussian, J. Vela, Y. Chen, J.A. Hollingsworth, V.I. Klimov, Nano Lett. 10 (2010) 2401.
[25] B.N. Pal, Y. Ghosh, S. Brovelli, R. Laocharoensuk, V.I. Klimov, J.A. Hollingsworth, H. Htoon, Nano Lett. 12 (2011) 331.
[26] J. Vela, H. Htoon, Y. Chen, Y.S. Park, Y. Ghosh, P.M. Goodwin, J.H. Werner, N.P. Wells, J.L. Casson, J.A. Hollingsworth, J. Biophotonics 3 (2010) 706.
[27] F. García-Santamaría, Y. Chen, J. Vela, R.D. Schaller, J.A. Hollingsworth, V.I. Klimov, Nano Lett. 9 (2009) 3482.
[28] J.M. Pietryga, D.J. Werder, D.J. Williams, J.L. Casson, R.D. Schaller, V.I. Klimov, J.A. Hollingsworth, J. Am. Chem. Soc. 130 (2008) 4879.
[29] H. Zhao, M. Chaker, D. Ma, J. Mater. Chem. 21 (2011) 17483.
[30] F. Li, D.I. Son, T.W. Kim, E. Ryu, S.W. Kim, S.K. Lee, Y.H. Cho, Appl. Phys. Lett. 95 (2009) 061911.
[31] L. Dworak, V.V. Matylitsky, V.V. Breus, M. Braun, T. Basché, J. Wachtveitl, J. Phys. Chem. C 115 (2011) 3949.
[32] N.P. Gurusinghe, N.N. Hewa-Kasakarage, M. Zamkov, J. Phys. Chem. C 112 (2008) 12795.
[33] S. Chakrabarty, K. Chakraborty, A. Laha, T. Pal, S. Ghosh, J. Phys. Chem. C 118 (2014) 28283.
[34] W. Ma, J.M. Luther, H. Zheng, Y. Wu, A.P. Alivisatos, Nano Lett. 9 (2009) 1699.
[35] K. Boldt, N. Kirkwood, G.A. Beane, P. Mulvaney, Chem. Mater. 25 (2013) 4731.
[36] B.-R. Hyun, Y.-W. Zhong, A.C. Bartnik, L. Sun, H.D. Abruna, F.W. Wise, J.D. Goodreau, J.R. Matthews, T.M. Leslie, N.F. Borrelli, ACS Nano 2 (2008) 2206.
[37] L. Jin, H. Zhao, D. Ma, A. Vomiero, F. Rosei, J. Mater. Chem. A 3 (2015) 847.
[38] Y. Chen, J. Vela, H. Htoon, J.L. Casson, D.J. Werder, D.A. Bussian, V.I. Klimov, J.A. Hollingsworth, J. Am. Chem. Soc. 130 (2008) 5026.
[39] H. Zhao, M. Chaker, N. Wu, D. Ma, J. Mater. Chem. 21 (2011) 8898.
[40] H. Zhao, T. Zhang, M. Chaker, D. Ma, J. Nanosci. Nanotechnol. 10 (2010) 4897.
[41] B.D. Mangum, S. Sampat, Y. Ghosh, J.A. Hollingsworth, H. Htoon, A.V. Malko, Nanoscale 6 (2014) 3712.
[42] S.J. Pennycook, P.D. Nellist, Scanning Transmission Electron Microscopy, Springer, New York Dordrecht Heidelberg London, 2011.
[43] M.M.J. Treacy, A. Howie, C.J. Wilson, Philos. Mag. A 38 (1978) 569.
[44] A. Howie, J. Microsc. 117 (1979) 11.
[45] V. Pinchetti, F. Meinardi, A. Camellini, G. Sirigu, S. Christodoulou, W.K. Bae, F. De Donato, L. Manna, M. Zavelani-Rossi, I. Moreels, V.I. Klimov, S. Brovelli, ACS Nano 10 (2016) 6877. http://dx.doi.org/10.1021/acsnano.6b02635.
[46] S. Christodoulou, G. Vaccaro, V. Pinchetti, F. De Donato, J. Grim, A. Casu, A. Genovese, G. Vicidomini, A. Diaspro, S. Brovelli, J. Mater. Chem. C 2 (2014)

3439.
[47] a) M. Murayama, T. Nakayama, Phys. Rev. B 49 (1994) 4710;
b) Z. Bandić, Z. Ikonić, Phys. Rev. B 51 (1995) 9806.
[48] a) H.-L. Chou, C.-H. Tseng, K.C. Pillai, B.-J. Hwang, L.-Y. Chen, J. Phys. Chem. C 115 (2011) 20856;
b) J. Ouyang, J.A. Ripmeester, X. Wu, D. Kingston, K. Yu, A.G. Joly, W. Chen, J. Phys. Chem. C 111 (2007) 16261.
[49] K. Gopidas, M. Bohorquez, P.V. Kamat, J. Phys. Chem. 94 (1990) 6435.
[50] a) B.-R. Hyun, A. Bartnik, L. Sun, T. Hanrath, F. Wise, Nano Lett. 11 (2011) 2126;
b) H. Zhao, Z. Fan, H. Liang, G. Selopal, B. Gonfa, L. Jin, A. Soudi, D. Cui, F. Enrichi, M. Natile, I. Concina, D. Ma, A.O. Govorov, F. Rosei, A. Vomiero, Nanoscale 6 (2014) 7004.
[51] Y. Justo, P. Geiregat, K.V. Hoecke, F. Vanhaecke, C. De Mello Donega, Z. Hens, J. Phys. Chem. C 117 (2013) 20171.
[52] T. Watanobe, K. Honda, J. Phys. Chem. 86 (1982) 2617.
[53] J.L. Blackburn, D.C. Selmarten, A.J. Nozik, J. Phys. Chem. B 107 (2003) 14154.
[54] T.R. Senty, S.K. Cushing, C. Wang, C. Matranga, A.D. Bristow, J. Phys. Chem. 119 (2015) 6337.
[55] R. van de Krol, M. Grätzel, Photoelectrochemical hydrogen production, New York, USA, *Springer*, 2011 ISBN 9781461413806.
[56] I. Mora-Sero, S. Gimenez, F. Fabregat-Santiago, R. Gomez, Q. Shen, T. Toyoda, J. Bisquert, Acc. Chem. Res. 42 (2009) 1848.
[57] X. Zhang, Y. Zhang, H. Wu, L. Yan, Z. Wang, J. Zhao, W.Y. William, A.L. Rogach, RSC Adv. 6 (2016) 17029.
[58] J. Tang, K.W. Kemp, S. Hoogland, K.S. Jeong, H. Liu, L. Levina, M. Furukawa, X. Wang, R. Debnath, D. Cha, Nat. Mater. 10 (2011) 765.
[59] W. Sheng, B. Sun, T. Shi, X. Tan, Z. Peng, G. Liao, ACS Nano 8 (2014) 7163.
[60] H.G. Zhao, D.F. Wang, T. Zhang, M. Chaker, D.L. Ma, Chem. Commun. 46 (2010) 5301.
[61] A.M. Dennis, B.D. Mangum, A. Piryatinski, Y.S. Park, D.C. Hannah, J.L. Casson, D.J. Williams, R.D. Schaller, H. Htoon, J.A. Hollingsworth, Nano Lett. 12 (2012) 5545.

Lei Jin received her Bachelor Degree in Applied Physics from Tianjin University (2012), China. She obtained Master Degree at the Institut National de la Recherche Scientifique (INRS, Canada), conducting research on quantum dot solar cells (2013). She is currently working as a Ph.D student at INRS, developing QDs based photoelectrochemical electrode for H_2 generation.

Andrea Camellini obtained his Master degree in Engineering Physics in October 2014 , degree course: Photonics and Nano-optics, from Politecnico di Milano. He is currently a PhD Candidate in Physics at Politecnico di Milano under the supervision of Prof. Margherita Zavelani-Rossi. His research focuses on ultrafast spectroscopy of low-dimensional system, in particular colloidal core shell nanocrystals and two dimensional transition metal dichalcogenides.

Xin Tong obtained his MS degree from Northwest University (China) in 2011. Currently, he is a lecturer at Guizhou Normal University and a PhD student at INRS. His research interests mainly focus on electrochemical applications of nanostructured materials.

Gianluca Sirigu was born in Cagliari (Italy) in 1986. In 2012 he received a master degree in Physics from the Università degli Studi di Cagliari. Now he is finishing his PhD in Physics in Politecnico di Milano. His research activity is focused on nonlinear optics, ultrafast spectroscopy and their application for the study of linear and nonlinear optical properties of nanostructures.

Andrea Parisini is a senior researcher at the IMM Institute of the National Research Council (CNR) in Bologna. He received his PhD in Material Science from the University of Grenoble in 1989. As an electron microscopist, his works have concerned various aspects of the structural characterization of semiconductors and carbon-related materials whereas, more recently, he has focused his activity on quantitative methods in Z-contrast scanning transmission electron microscopy.

Giuseppe Nicotra is staff researcher at the headquarters of the IMM-CNR of Catania, and director of the Sub-A resolution transmission electron microscopy laboratory. He got the the PhD in materials science at University of Catania working also as visitor researcher at the University of California at Davis and the National Center for Electron Microscopy, Berkeley (USA). His initial works spans from the study of processes and synthesis of nanostructures for applications both microelectronics and photonics. Recently he is involved into the study of new innovative two-dimensional (2D) materials, such as Graphene, Silicene and Phosphorene, at atomic level.

Corrado Spinella received his Dr. degree in Physics in 1985. In 1989 he joined as researcher the Istituto Nazionale di Metodologie e Tecnologie per la Microelettronica (IMETEM) of the Italian National Research Council (CNR). From 1999 to 2001 he was Director of IMETEM and in 2002 he moved as senior researcher to the Institute for Microelectronics and Microsystems (IMM). Since 2008 to 2014 he was Director of IMM. At the present he is President of the National Technological District “Sicilia Micro Nanosistemi” and Director of the Department of Physics and Technology of Matter - CNR. His research activity is in the field of new materials and processes for micro– and nanoelectronics: front–end processing for ultra large scale Si technology; Si–based optoelectronics; science and technology of silicon carbide for RF or power electronics; novel memory devices based on silicon nanocrystals; advanced techniques, based on transmission electron microscopy, for characterization of nanostructured materials. He is co–author of more than 230 scientific papers and of several international patents.

Haiguang Zhao is a Research Associate of the INRS Centre for Energy, Materials and Telecommunications, Quebec University, Varennes (QC) Canada. He received MSc degree (2007) from Zhejiang University and PhD degree (2012) from INRS, Quebec University. He is currently a sub-group leader in Prof. Rosei’s group in INRS. His research interests focus on the synthesis of semiconductor materials (including metal oxide, quantum dot and perovskite) for solar energy applications, such as solar cell, luminescent solar concentrator and solar-driven water splitting.

Prof. Shuhui Sun received his MSc/Ph.D degree from Chinese Academy of Sciences (CAS) in 2004, and then continued his research at INRS and the University of Western Ontario (UWO), both in Canada. Dr. Sun is now an associate professor at the Institut National de la Recherche Scientifique (INRS)-Energy, Materials, and Telecommunications, Canada. He has been awarded the Canada Governor General's Gold Medal. His current research interests mainly focus on the development of multifunctional nanomaterials and catalysts for energy conversion and storage, and environment.

Vittorio Morandi, Ph.D in Physics at the University of Bologna, is Senior Scientist and Head of the CNR-IMM Bologna Section. His research activities concern the development of advanced electron microscopy techniques, with a particular focus on SEM and STEM at low and high energy, the structural characterization of nano-scale materials, in particular low-dimensional carbon allotropes, and synthesis, characterization and technological processing and integration of graphene-based materials. He is author of more than 80 papers in high impact international journals, and has participated to about 50 international conferences with oral presentations, with talks on SEM, STEM, graphene characterization and exploitation.

Margherita Zavelani-Rossi received the M.S. degree in Electronic Engineering and the PhD in Physics at the Politecnico di Milano (Italy), she spent one year at the Laboratoire d'Optique Appliquée (ENSTA-CNRS-Ecole Polytechnique, France) and then worked at the Politecnico di Milano where she is now Associate Professor at the Energy Department. She is lecturer of physics courses, co-author of more than 70 international articles, 2 book chapters and of an international patent. Her main research interests focus on the generation of short laser pulses (fs-regime) and on the ultrafast spectroscopy of organic materials and of semiconductor and metallic nanoparticles.

Federico Rosei is Professor and Director of the INRS Centre Énergie, Matériaux et Télécommunications, Varennes (QC) Canada. He holds the UNESCO Chair in Materials and Technologies for Energy Conversion, Saving and Storage and the Senior Canada Research Chair in Nanostructured Materials. He received MSc and PhD degrees from the University of Rome “La Sapienza” in 1996 and 2001, respectively. He has received several awards and is Fellow/Member of many prestigious societies and academies, including the Royal Society of Canada, the European Academy of Sciences, the American Physical Society, the Chinese Chemical Society (Honorary), the American Association for the Advancement of Science, SPIE, the Canadian Academy of Engineering, ASM International and the Engineering Institute of Canada.

Alberto Vomiero is Chair Professor in Experimental Physics at the Department of Engineering Sciences and Mathematics, Luleå University of Technology, Sweden since October 2014. He was awarded his PhD in Electronic Engineering from the University of Trento in 2003 and his Degree in Physics from the University of Padova in 1999. His main interests are in composite nanomaterials for environmental applications. He is former Marie Curie International Outgoing Fellow of the European Commission, Fellow of the Swedish Foundations, of the Royal Society of Chemistry (UK), of the Institute of Physics (UK) and of the Institute of Nanotechnology (UK), former chair of the Italian section of the American Nano Society and member of the Global Young Academy.